ADVANCED MATERIALS
www.advmat.de

Implanted Carbon Nanotubes Harvest Electrical Energy from Heartbeat for Medical Implants

Arjang Ruhparwar, Anja Osswald, Heewoo Kim, Reza Wakili, Jan Müller, Nikolaus Pizanis, Fadi Al-Rashid, Ulrike Hendgen-Cotta, Tienush Rassaf, and Seon Jeong Kim**

Reliability of power supply for current implantable electronic devices is a critical issue for longevity and for reducing the risk of device failure. Energy harvesting is an emerging technology, representing a strategy for establishing autonomous power supply by utilizing biomechanical movements in human body. Here, a novel "Twistron energy cell harvester" (TECH), consisting of coiled carbon nanotube yarn that converts mechanical energy of the beating heart into electrical energy, is presented. The performance of TECH is evaluated in an in vitro artificial heartbeat system which simulates the deformation pattern of the cardiac surface, reaching a maximum peak power of 1.42 W kg^{-1} and average power of 0.39 W kg^{-1} at 60 beats per minute. In vivo implantation of TECH onto the left ventricular surface in a porcine model continuously generates electrical energy from cardiac contraction. The generated electrical energy is used for direct pacing of the heart as documented by extensive electrophysiology mapping. Implanted modified carbon nanotubes are applicable as a source for harvesting biomechanical energy from cardiac motion for power supply or cardiac pacing.

1. Introduction

Cardiac implantable electronic devices (CIEDs) such as implantable pacemakers and cardioverter-defibrillators, neurostimulators, and mechanical circulatory support devices have contributed substantially to the treatment of various cardiovascular diseases, including arrhythmia, ventricular fibrillation, and heart failure.[1] Cardiac pacemakers detect abnormal heart activity and deliver electrical pulses to cardiac tissue for restoring normal cardiac rhythm.[2] CIEDs are able to replace the function of our body's inherent pacemaker. While the technology of medical devices is in rapid development, power supply remains a critical issue. Currently, a lithium-ion battery is used as the power source for CIEDs. Its finite lifespan creates a risk of device malfunction due to battery depletion.[3] Replacement of the device every 4–10 years is unavoidable posing a risk for the patient with each surgery.[4–6] Many approaches searching for biological pacemaker alternatives have achieved good results in preclinical trials but are not yet alternatives in clinical practice.[7] The reliable functionality of modern pacemakers due in part to the decades of experience as well as the programming options for different pacing modalities pose a huge advantage, making the search for alternative energy sources essential. In order to overcome the limitations caused by the batteries of the CIEDs, efforts have focused on the improvements of energy sources for avoiding frequent replacement surgery as well as to reinforce its biocompatibility.[8] Self-powered energy harvesters that generate energy from the environment are regarded as promising tools of sustainability, since limited device

A. Ruhparwar, A. Osswald, J. Müller, N. Pizanis
Department of Thoracic and Cardiovascular Surgery
West-German Heart and Vascular Center Essen
University of Duisburg-Essen
Hufelandstraße 55, 45147 Essen, Germany
E-mail: anja.osswald@uk-essen.de

A. Ruhparwar
Department of Cardiothoracic
Transplantation and Vascular Surgery
Hannover Medical School
30625 Hannover, Germany

The ORCID identification number(s) for the author(s) of this article can be found under https://doi.org/10.1002/adma.202313688

DOI: 10.1002/adma.202313688

H. Kim, S. J. Kim
Department of Biomedical Engineering
National Creative Research Initiative Center for Self-Powered Actuation
Hanyang University
Seoul 04763, South Korea
E-mail: sjk@hanyang.ac.kr

R. Wakili, F. Al-Rashid, U. Hendgen-Cotta, T. Rassaf
Department of Cardiology and Vascular Medicine
West-German Heart and Vascular Center Essen
45147 Essen, Germany

R. Wakili
Department of Cardiology and Vascular Medicine
University Hospital Frankfurt
Goethe University
60590 Frankfurt, Germany

lifespan becomes of less concern. Continuous, constant, and periodic movements of body parts or organs like a heart muscle, diaphragm, blood flow, or contracting muscles represent attractive sources for energy harvesting owing to their infinite and inexhaustible characteristics during our lifetime. In particular, harvesting energy from the heartbeat with the capability of producing ≈1 W of mechanical performance is promising due to its periodic nature and large changes in muscle conformation.[9,10] Various types of energy harvesters with piezoelectric or triboelectric elements have been designed and applied to the cardiac environment. The harvested electrical energy has been directed to diverse applications such as powering CIEDs, pacing the heart directly, or monitoring cardiac status.[11–16] However, these devices are either too rigid or bulky and do not deliver the necessary amount of energy required for CIEDs.[17]

Twistrons are a new type of electrochemically driven energy harvester made up of carbon nanotubes (CNT). Twistrons have a stretchable coiled structure, transforming mechanical energy of length deformation to electricity by inducing capacitance change in the electrolyte without the need for external bias voltage.[18] This approach is based on this emerging technology to convert generally ambient and wasted energy to useful electrical energy and mechanical power. Twistrons have been woven into a textile to harvest energy from the bending motion of a knee, showing the possibility of a wearable energy harvesting device.[19] The biocompatibility and working principle of a Twistron allowed it to operate as a gastric movement sensor, which generates electricity according to simulated periodic gastric deformation.[20] Recent research reported of high performances of Twistrons: a coiled CNT harvester embedding reduced graphene oxide generates a high power density of up to 730 W kg^{-1} at 1 Hz, and a threeplied CNT harvester has a high energy efficiency of up to 17.4% at 0.1 Hz.[21,22] The high performance of Twistrons and the fiber shape of the CNT electrodes have advantages as an energy source for wearables or in vivo. This power enhancement underscores the rapid development and high dynamic in this field.

In our study, a novel energy harvesting device consisting of coiled CNT yarn is demonstrated to convert mechanical energy into electricity (I). The performance of this device was evaluated in an in vitro artificial heartbeat system which simulates the deformation pattern of the cardiac surface under various conditions that mimic a real human heart, allowing the detailed analysis of the properties of the generated electricity (II). In a next step, an in vivo preclinical porcine model was established with the aim to demonstrate the feasibility of Twistrons for continuously generating electrical energy from cardiac mechanical activity and to serve as a cardiac pacemaker by direct autogenic stimulation of the heart (proof-of-concept study).

2. Experimental Section

2.1. Device Design and Characteristics

2.1.1. Fabrication of Twistron Energy Harvester

To fabricate a working electrode, a precursor CNT sheet (length: 30 cm, width: 6 cm) was drawn from the multi-walled CNT forest produced by chemical vapor deposition (CVD) process. The length of the drawn CNT sheet follows the direction of the CNT alignment. Then the CNT sheet was rolled into a hollow cylindrical shape, with its axis matching to the direction of length. The cylindrical CNT sheet was suspended vertically to a rotational motor and a load of 107 MPa was applied to the bottom of the cylinder. A twist was exerted on the CNT cylinder in one regular direction by the rotational motor. During twisting, the cylindrical form of the CNT sheet changed to the shape of the twisted yarn. After 26 turns cm^{-1}, this densely twisted CNT yarn transformed to a coiled CNT yarn by exerting more twist in the same direction of rotation with rotational motor. In order to confine a stretching range of the coiled CNT yarn to 30%, the load was replaced to a lighter load of 15.4 MPa. After coils were completed along the entire length with the total twist density of 61 turns cm^{-1}, a fully coiled CNT yarn was then reversely twisted around 8% of the total twisting density under the same coiling load for higher flexibility and performance. Untwisting process resulted in the final coiled CNT yarn having a spring index of 0.53, having ability to stretch to around 30%.

A counter electrode was made by the same process of fabrication of CNT yarn. Because a counter electrode should have sufficiently larger electrochemical accessible area than that of the working electrode, four times larger amount of CNT was used for fabrication of counter electrode. Instead applying large load and twisting densely like fabrication of working electrode, smaller load around 1 or 2 MPa was applied, and cylindrical CNT sheet is loosely twisted to secure large surface area.

2.1.2. Fabrication of TECH

In order to contain the whole Twistron system in a compact device, the CNT coil working electrode and twisted CNT yarn counter electrode were placed together in the flexible silicone tube. The nylon knit surrounded the counter electrode to separate the two electrodes physically, but simultaneously make them share the electrolyte. Two 3D-printed support parts with small holes for easy suture on the cardiac surface were located at each end of the device, respectively, and fixate the ends of electrodes. A cylindrical silicone was used for the device body, and its flexible and biocompatible characteristics allowed TECH to be stretched smoothly along the movement of the biological cardiac surface.[23] After two electrodes were located inside the silicone tube, TECH is filled with 0.15 M NaCl aqueous electrolyte, which has a similar concentration to a physiological saline solution (0.9% NaCl). Then the silicone tube was entirely sealed by its ends being connected to the support parts by applying epoxy, resulting in a form of a hollow and closed cylindrical silicone container with whole Twistron system being contained.

2.1.3. Electrochemical Characterization

Electrochemical performance of TECH was measured by using a Gamry potentiostat (reference 600+). OCV, SCC, and power were measured in a two-electrode system consisting of a coiled CNT yarn as a working electrode and a twisted CNT yarn as a counter electrode. To measure a capacitance and following OCV of a Twistron energy harvester, cyclic voltammetry and OCV were measured in a three-electrode system, where a working electrode

was a coiled CNT yarn, a counter electrode was a twisted CNT yarn, and a reference electrode was Ag/AgCl.

2.2. In Vitro Artificial Heartbeat System

For the implementation of the movement of a left ventricle's (LV) outer surface, a circular and hollow frame with the size of covering the balloon surface connected to a stepping motor via a crank regularly exerts pressure vertically on a water-filled balloon so that the part of the exposed balloon surface inside the frame expands when being pressed by the frame. Then, in order to make the balloon's movement resemble the motility of LV during a cardiac cycle, one expansion and contraction cycle was divided into 4 sections, each assigned different rotation angles and speeds by programming the stepping motor to mimic the complicated strain motion of the heart (Figure S1, Supporting Information). In consequence, TECH was able to conformally adhere to a balloon's surface and repeat elongation and contraction according to the GLS pattern of the surface's movement produced by the in vitro artificial heartbeat system.

2.3. In Vivo Application in a Porcine Model

2.3.1. Large Animal Model Experiment

The experimental protocol was reviewed and approved by the Committee on Research Animal Care, Land Nordrhein–Westfalen (Landesamt für Natur, Umwelt und Verbraucherschutz Nordrhein-Westfalen, AZ 81-02.04.2019.A465). All animals received humane care in compliance with the "Principles of Laboratory and Animal Care" and the Guide for the Care and Use of Laboratory Animals, prepared by the Institute of Laboratory Animal Resources and published by the National Institutes of Health (NIH Publication No. 86-23, revised 1996). The ARRIVE guidelines 2.0 was followed.

Ten female German Landrace pigs (42 ± 4 kg) were utilized in this study. The pigs were sedated with an intramuscular injection of atropine (0.02–0.05 mg kg^{-1}), azaperone (0.05 mg kg^{-1}), and ketamine (0.3 mg kg^{-1}). After insertion of an intravenous catheter into the ear vein, propofol 2% was administered. The animal was placed on the operating table and endotracheally intubated. Mechanical ventilation (Dräger Oxylog 3000 plus) was performed in bilevel positive airway pressure ventilation mode with standard settings with a positive end-expiratory pressure of 5 cm H_2O, peak inspiratory pressure of 20 cm H_2O, and a respiratory rate of 12 min^{-1}. The settings were adjusted according to arterial blood gas analysis (Radiometer, Copenhagen, Denmark). Anesthesia was maintained with propofol 2% (7 mg kg h^{-1}), midazolam 0.5% (0.3 mg kg h^{-1}), and fentanyl (0.015 mg kg h^{-1}). Hemodynamic parameters were constantly monitored by invasive blood pressure measurement, as well as a 12-lead ECG. Catheter access was performed by 7 and 9 French sheaths inserted in the jugular vein (surgical cut-down) and an 8 French and 9 French sheaths into the left and right femoral artery and a 8 French sheath into a femoral vein (percutaneous access) (Figure S2, Supporting Information). A lateral thoracotomy was performed, and the heart was exposed by pericardiectomy. To reduce arrhythmic events, 300 mg of amiodarone was administered. As in standard epicardial pacemaker implantation in the clinical setting, the stretchable soft CNT were sutured onto the myocardial surface of the left ventricle apex with 4-0 monofilament nonresorbable sutures. To evaluate energy production, the wires were connected to an oscilloscope and measurements with different numbers of devices were performed for a maximum of 45 min in order to maintain the hemodynamic stability of the sensitive animals during anesthesia and surgery.

2.3.2. Cardiac Pacing

For cardiac pacing the wires from working and counter electrodes of TECH were inserted into the ventricle at a distance of ≈1 cm and fixated by 5-0 monofilament suture. To detect premature ventricular contractions (PVCs), heart rate had to be reduced. With administration of esmolol (500 µg kg min^{-1} for 1 min, maintenance dose of 50 µg kg min^{-1}) as well as adenosine boli (6–18 mg) only a minor heart rate reduction was achieved. Therefore, atrioventricular (AV) node ablation was performed during mapping studies.

2.3.3. Mapping Studies

During procedure, a steerable decapolar catheter was placed in coronary sinus (CS). The Orion multipolar basket catheter and Rhythmia system (both Boston Scientific, Marlborough, MA) were used for the LV mapping. In addition, a pace/sense catheter was placed in the RV via venous access. A local activation (LAT) map was generated with automatic standard beat acceptance criteria based on the annotations-algorithm: (1) cycle length (CL) variation, (2) activation time difference variations between the CS EGMs, (3) propagation reference (ΔR), (4) respiration, (5) QRS morphology "favorite beat" (ECG), (6) mapping catheter movement, (7) electrogram stability compared to last beat, (8) tracking quality, and (9) window.

2.3.4. Tissue Harvesting

After euthanasia with 20% potassium chloride, explantation of the heart was performed (Figure S3, Supporting Information). Tissue samples were obtained from the left ventricle, interventricular septum, and left atrium to evaluate potential structural damage to the cardiac tissue (Figure S4, Supporting Information). For H&E staining, samples of the left-ventricle were fixed in paraformaldehyde 4%, embedded in paraffin and sectioned in 5 µm sections. The combination of hematoxylin, which stains nuclei blue, and eosin which stains the extracellular matrix and the cytoplasm pink, provide a good overview of the tissue sample.

Tissue processing for transmission electron microscopy (TEM) was performed as previously described.[24] In brief, the samples were transferred into a primary fixative (2% formaldehyde, 2.5% glutaraldehyde, and 2×10^{-3} M $CaCl_2$ in 0.15 M cacodylate buffer) and incubated for at least 3 h at room temperature. After postfixation, the samples were dehydrated in a series of ethanol solutions, embedded in Durcupan followed by polymerization for 72 h at 60 °C. Semi-thin sections were first evaluated with light microscopy The embedded tissue was cut into

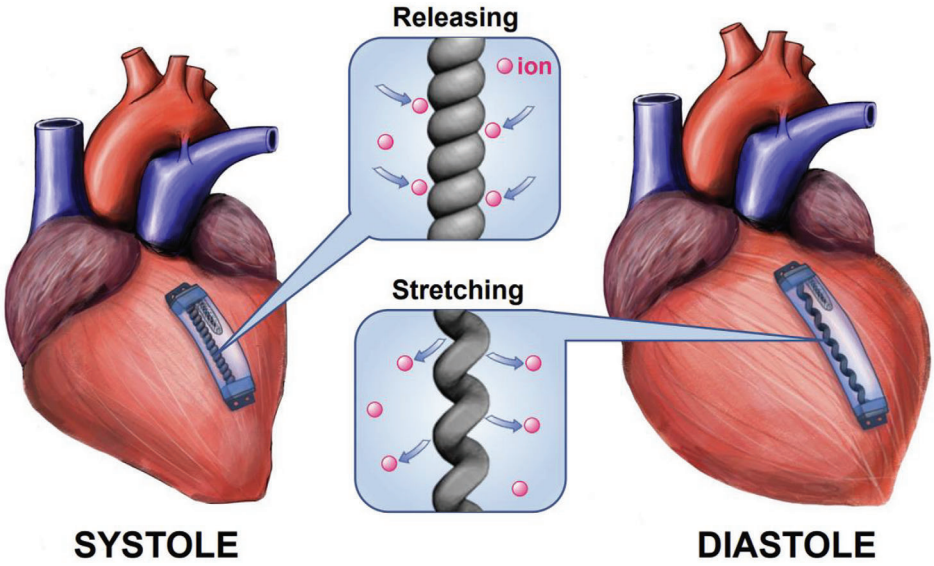

Figure 1. Schematic illustration of a Twistron energy cell harvester (TECH) on a cardiac surface and its principle to harvest electricity from heartbeat motility. The dimensional changes of the cardiac surface of a left ventricle (LV) during the repeated heartbeat cause the TECH conformally on the surface of the heart to periodically stretch and contract. Consistent variations in the length of the coiled carbon nanotube (CNT) yarn resulting from this induce an ion migration around it, causing the change in capacitance. Therefore, these dimensional changes are converted to electricity by the Twistron.

ultrathin sections (55 nm) and analyzed using a LaB6 cathode-equipped JEM 1400Plus (JEOL, Ltd., Tokyo Akishima, Japan) instrument at 120 kV. Digital images were acquired with a CMOS camera with 4096 × 4096 pixels (TemCam-F416, TVIPS, Gauting, Germany).

3. Results

3.1. Device Design and Characteristics

3.1.1. Basic Function

When the TECH was stretched at the heart's diastolic phase, the capacitance of the stretched working electrode, the coiled CNT yarn inside the TECH, decreased due to the high proximity between CNT bundles. All TECHs exhibited this function. The mechanism of how a TECH generates electrical energy from the periodic mechanical heartbeat movement is shown in **Figure 1** Increase in the proximity of the bundles reduced space for charged ions which resulted in voltage increase according to the relationship that the amount of charge (Q) is determined as the product of capacitance (C) and voltage (V) ($Q = CV$)[18] (Figure S5, Supporting Information). **Figure 2**A shows the structure of cardiac implantable TECH, encapsulated in a flexible and biocompatible silicone tube.

3.1.2. Optimal Spring Index

We tested different spring index (SI) conditions of the coiled CNT yarn working electrode with respect to both maximum open-circuit voltage (OCV) changes and strain range (Figure 2B). A coiling load of 15.4 MPa was used for fabricating Twistron with a SI of around 0.53, which limited its stretching up to 30% (Figure S6, Supporting Information). With this SI, the Twistron stretched safely and also generated the best performance in the target strain range compared to the other Twistrons having different spring indices even though their performances at their respective maximum strain are on the same level around 120 mV of OCV (Figure 2B). For an SI of 0.38 (lower than 0.53), the maximum strain range of the Twistron was only 15% therefore not performing fully within the entire target strain range. Twistrons having a SI higher than 0.53 could be stretched over the targeted range, whereas the performance in the target strain range was low. Although the stretching range of the Twistron with SI of 0.77 was 50%, the maximum peak-to-peak OCV at the target strain range was only 87.9 mV compared to 122.3 mV of peak-to-peak OCV generated by the Twistron with 0.53 of SI at the same strain range (30%), Twistrons having SI higher than 0.53 was not appropriate in terms of performance. In addition, by adjusting the SI of Twistrons and eventually its optimal working condition, it has the potential to be applied to other parts than the heart of the periodically moving body like the diaphragm, stomach to harvest various biomechanical energy with the most optimal performance.

3.1.3. Device Encapsulation

Figure 2C shows the 20% applied sinusoidal tensile strain and the corresponding generated OCV of the identical coiled CNT yarns under two different conditions in the experimental setup which was the two-electrode system in the electrolyte bath using a platinum mesh as a counter electrode and in the fully packaged TECH. It turned out that the abilities to generate OCV before and after being encapsulated into the compact device had a negligible difference, that their peak-to-peak OCV is 91.7 and 87.2 mV,

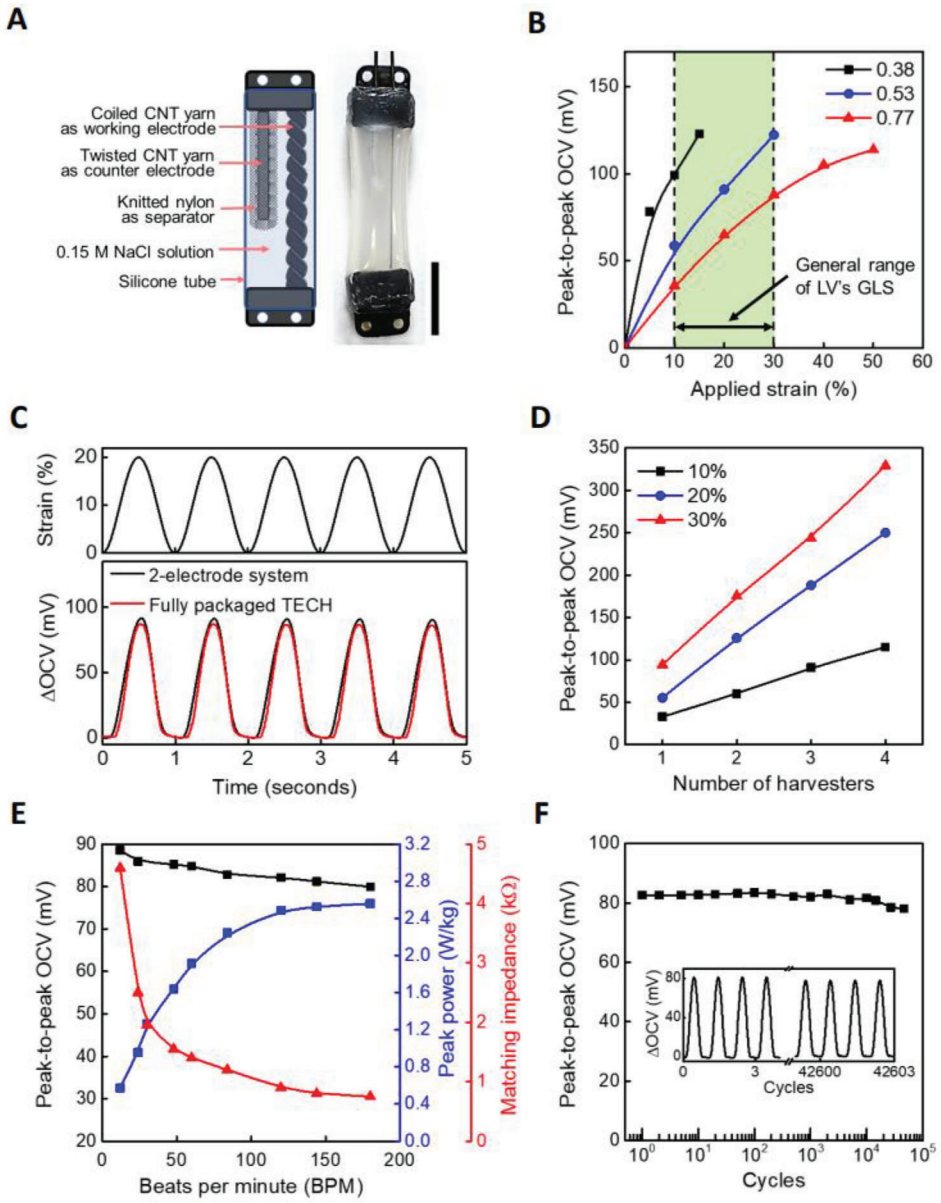

Figure 2. Characteristics of a TECH as a cardiac implantable energy harvester. A) Illustration and photograph of a structure of a TECH (scale bar, 1 cm). B) Spring index optimization of the CNT coiled yarn regarding the general range of LV's global longitudinal strain (GLS). C) A sinusoidally applied tensile strain of 20% and resulting change in open-circuit voltage (OCV) generated by Twistron before (black) and after (red) being fabricated into a fully packaged TECH. D) Peak-to-peak OCV according to the applied strain values and the number of connected harvesters in series. Sinusoidal strain of 1 Hz was applied. E) Frequency dependence of peak-to-peak OCV (black squares), peak power (blue circle), and matching impedance (red triangles). F) Peak-to-peak OCV during ≈50 000 stretch-and-release cycles to 20% sinusoidal strain at 1 Hz. (Inset) Comparison of the OCV at the first three cycles and after ≈42 600 cycles.

respectively, showing that there was no serious degradation of performance due to encapsulation.

3.1.4. Multiple Device Combination

In order to enhance the performance for more diverse applications, the connection between several TECHs was tested. As shown in Figure 2D and Figure S7 (Supporting Information) performance became higher with larger strain and more TECHs involved in the connection. When four TECHs were connected in serial or parallel and stretched sinusoidally to 30%, around 350 mV of maximum peak-to-peak OCV and 230 μA of maximum peak short-circuit current (SCC) are achieved respectively. The electrical outputs of TECH depending on stretching frequency were measured considering a diverse range of beating frequency of human heart with 20% sinusoidal strain applied. Figure 2E shows that peak-to-peak OCV tended to decrease slightly as beats

per minute (BPM) increased because rapid stretch and release prohibits enough ion intrusion and extrusion to and from coiled CNT yarn, however, the decrease in OCV was not at a critical degree.

If four TECHs were serially connected and stretched with 1 Hz, 20% applied strain, 0.338 μJ of energy per cycle is produced at 6 kΩ of load resistance (Figure S8, Supporting Information), which is similar to the pacing threshold energy of the human heart (0.377 μJ) and higher than that of the porcine heart (0.262 μJ), showing the potential of its utility as a cardiac stimulator which delivers electrical energy harvested from the physical movement of the heart to heart itself in order to induce the normal heart rhythm as the pacemaker does.[25,26] The power generated from TECH was also calculated with a measured matching impedance at various stretching frequencies. Both peak power and average power had a tendency to increase as BPM became faster (Figure 2E and Figure S9, Supporting Information). Because TECH's internal impedance is inversely affected by the stretching frequency, the matching impedance diminishes as BPM becomes more rapid, resulting in increasing power following the relationship that power generated from it (P) was calculated as the square of peak voltage (V) divided by the load resistance (R) ($P = V2/R$). The matching impedance is the inherent impedance of a Twistron, where the Twistron can produce its maximum power. Generated power tends to firstly become higher as load resistance increases and eventually start to decline after producing the maximum power at one point where the load resistance and inherent impedance of Twistron become identical, which is called the matching impedance (Figure S10, Supporting Information).

3.1.5. Durability Testing

Durability and stability are essential to realizing a sustainable power source for the continuous operation of implantable medical devices. A cyclic test was conducted under the condition of 20% sinusoidal strain at 1 Hz (Figure 2F). During a 50 000 iterative stretch-and-release cycle, the retention rate of peak-to-peak OCV is about 94% as well as its elastic but sturdy structure remains intact, demonstrating the possibility of the long-term sustainable biomechanical energy harvester. Since this energy harvesting is achieved through a reversible mechanical-electrochemical reaction inside the silicone container, a semi-permanent lifespan in vivo is expected, but additional observation is needed to address concerns about physical damage to the CNT electrode or silicone container.

3.2. In Vitro Artificial Heartbeat System

Since a Twistron converts linear movements into electricity, the unique 2D strain pattern of a cardiac surface generated from the consecutive mechanical event of the cardiovascular system affects the output of the TECH. Therefore, an in vitro artificial heartbeat system that resembled the strain pattern of the target implant surface, specifically a global longitudinal strain (GLS) of LV's epicardium was designed and TECH was evaluated on this in vitro artificial heartbeat system.

Figures 3A and S1 (Supporting Information) show how an in vitro artificial heartbeat system operates by adjusting a pressure applied to a water-filled balloon and the resultant strain waveform of the balloon surface. Figure 3B is the 20% peak GLS strain waveform at 60 BPM applied on the balloon's surface simulated by an in vitro artificial heartbeat system and corresponding OCV and SCC generated by TECH, respectively. It was observed that the OCV waveform follows the applied strain pattern, and the SCC waveform has a phase difference of 90° compared to the voltage waveform.

Electrical performances of TECH were assessed on an in vitro artificial heartbeat system with consideration of the human heart's diverse conditions. Since each part of the LV surface has a variety of strain ranges of its own, TECH was tested with various strain values within the scope of the LV's epicardial GLS.[27] Figure 3C shows that the generated OCV was proportional to the applied strain while maintaining the basic waveform of GLS, representing the potential utility of TECH as a real-time cardiac monitoring sensor as well. Moreover, TECH was tested under conditions of various frequencies regarding actual human heart rate (Figure 3D and Figure S11, Supporting Information). Considering human heart rates, GLS stimuli with three different BPMs of 50, 80, and 130 are applied. As demonstrated in Figure 3D and Figure S11 (Supporting Information), a beating frequency is reflected in the OCV and SCC change as the frequency of the repeated pattern, showing TECH's ability to detect a heart rate by the generated voltage or current waveform by virtue of its energy harvesting characteristic that its performance was proportionally responsive to the exerted strain.

Power generation by TECH was also evaluated in an in vitro artificial heartbeat system. When 30% simulated GLS strain of 60 BPM was applied, maximum peak power of 1.42 W kg^{-1} and average power of 0.39 W kg^{-1} were generated at the matching impedance of 400 and 700 Ω, respectively (Figure 3E). In addition, power generated by TECH could be obtained at various BPMs in the range of human heart rate (Figure 3F; Figures S12 and S13, Supporting Information). It was observed that power and energy per cycle generated by TECH are dependent on the deformation frequency. Decline in matching impedance as increase in stretching frequency resulted in increasing power.[18] When 20% simulated artificial heartbeat GLS strain was applied, around 60 mV of peak-to-peak OCV was stably maintained despite the BPM change. In addition, peak power increased from 1.05 to 2.50 W kg^{-1}, average power also increased from 0.32 to 0.55 W kg^{-1}, and energy per cycle declined from 0.36 to 0.26 J kg^{-1} as the beating frequency becomes higher from 50 to 130 BPM. This implies that TECH can not only generate power from heartbeat movement over the whole range of human heart rate for providing power supply to CIEDs or stimulating the heart directly but also gain information about cardiac status like strain and beating frequency from the tendency of power generation related to these deformation properties.

3.3. In Vivo Application in a Porcine Model

To assess the possibility of a TECH to be implanted on the actual heart surface and generate electrical energy by converting cardiac surface deformation, an in vivo performance of the

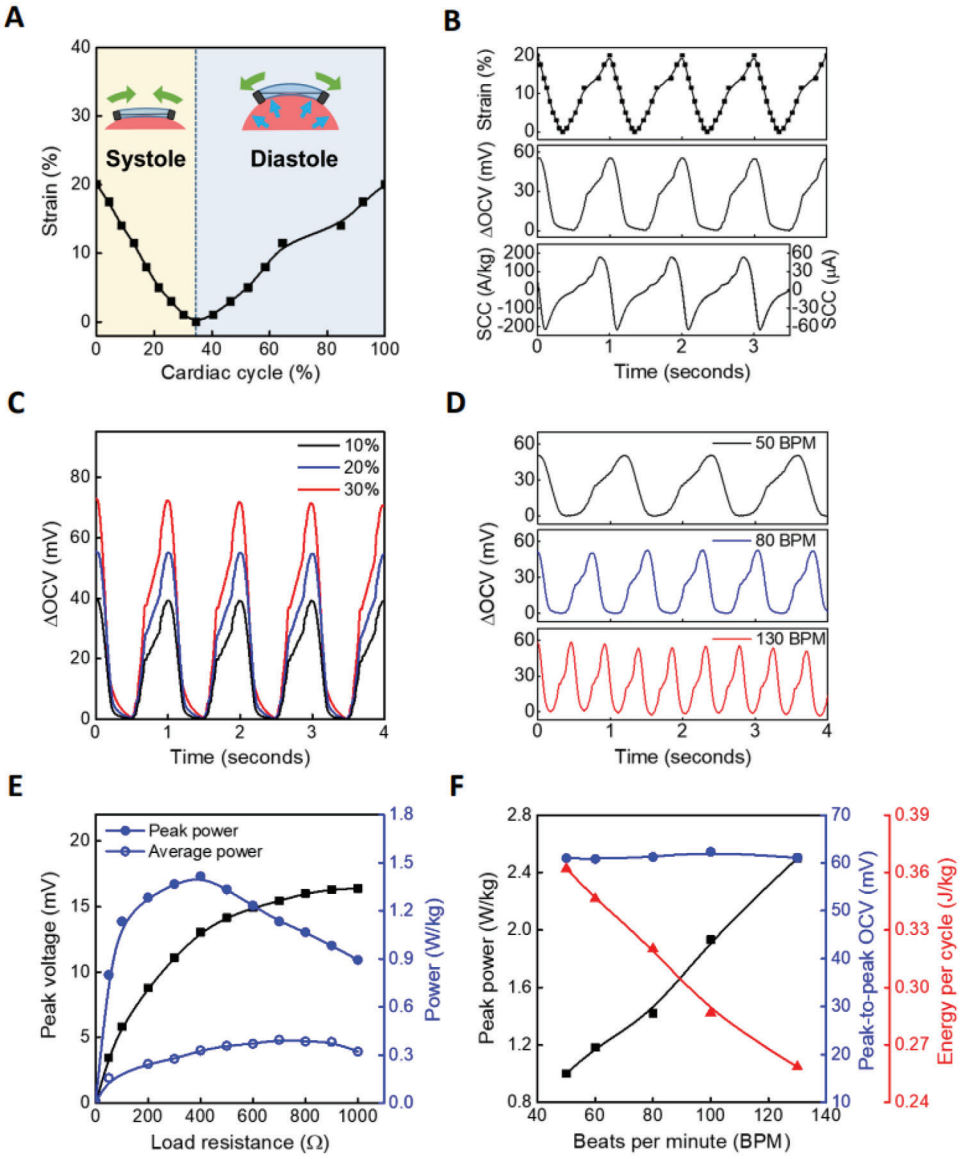

Figure 3. An in vitro artificial heartbeat system and the performance of TECH under the simulated motility of an actual human heart surface. A) One cycle of a strain change of the balloon surface which mimics the GLS of LV's epicardium generated by an in vitro artificial heartbeat system and (inset) the simplified working principle of it. B) 20% GLS strain waveform generated by an in vitro artificial heartbeat system and corresponding OCV and short circuit current (SCC) from TECH before (left) and after (right) normalization by the weight of a working electrode of TECH. C) OCV generations with various applied strains within the range of LV's GLS. D) OCV generations at various beating frequencies of 50 (sleeping), 80 (at rest), and 130 (exercising) beats per minute (BPM), with 20% of simulated GLS strain. E) Peak voltage (squares) and resulting peak power (blue, solid circles) and average power (blue, open circles) outputs of a TECH as a function of load resistance during artificial heartbeat with 30% of GLS strain at 60 BPM. F) Tendency of peak power (squares), peak-to-peak OCV (circles), and energy per cycle (triangles) depending on BPM of artificial heartbeat with 20% GLS strain.

TECH as an energy harvester and a potential cardiac pacemaker was evaluated in a porcine model (n = 10) (**Figure** 4A). During continuous heart beating, the length of TECH, sutured along to the LV's curved outer layer, changed simultaneously according to the periodic dimensional changes of the cardiac surface. Cardiac motion led to stretching of the flexible TECH, during the filling phase (diastole) and relaxation during blood ejection (systole) (Figure 4B,C). Voltage production was quantified by oscilloscope measurements, which were performed with a different number of devices connected in series (1–4 devices) to amplify the output (Figure 4A,D) in all animals/experiments. One device was able to yield a peak-to-peak OCV of ≈45 mV. A combined power of 60 mV was reached with two devices, 130 mV with three devices and a maximum of 140 mV with four devices (Figure 4D; Figure S14 and Movie S1, Supporting Information). The electrical output was in synchrony with the heartbeat and the connected ECG (Figure 4E). After ensuring that the TECH construct reliably generated energy through cardiac motion, a subsequent experiment was conducted to demonstrate that the devices are capable of electrically

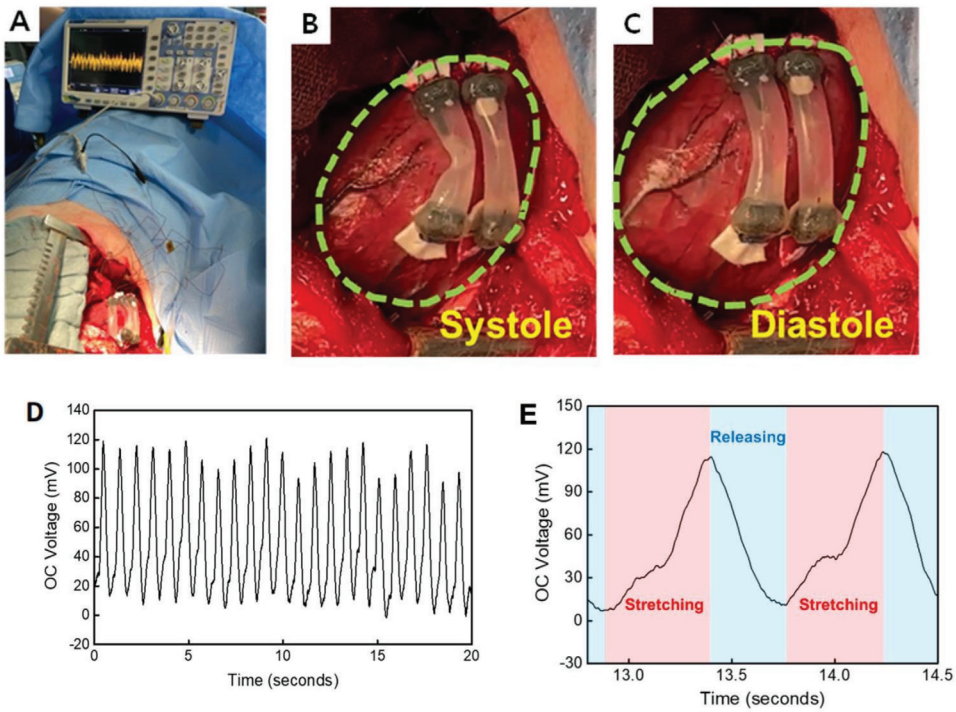

Figure 4. In vivo energy harvesting of TECH from heartbeat of a porcine model. A) The anesthetized swine was placed on its right side to perform a lateral thoracotomy and expose the heart. B,C) TECHs were placed between the apex of the heart and the valve level and generated electricity by repeated stretching by systole and diastole phases of the heart. The heart was beating in sinus rhythm. D) In vivo continuous output of OCV from four serially connected TECHs from the periodic heartbeat movement. E) A waveform of OCV according to the change of length of TECHs due to the movement of a heart.

stimulating the heart and thus can serve as a potential pacemaker.

3.3.1. Mapping Studies

To investigate the relationship between the electrical energy generated from TECH and a sufficient excitation of the myocardium a detailed activation mapping of the left ventricle was performed using the Rhythmia system (Rhythmia, Boston Scientific, Marlborough, MA). After insertion of cardiac catheters, a 3D high-density electro-anatomical maps of the heart chambers and anatomic reference points for AV node, sinus node were created using an Orion catheter (IntellaMap Orion, Boston Scientific, Marlborough, MA) (**Figure** 5A–C and Movie S2, Supporting Information). The mapping was assessed at the beginning before implantation of TECH. The two wires of the TECH each connected to working and counter electrodes respectively were placed into the myocardium of the left ventricle with a distance of ≈1 cm. During the series of experiments ($n = 10$) a workflow for decrease of spontaneous heart rate was established aiming to allow spontaneous ectopic heart beating generated by autogenic electrical transfer by the TECH device. For reduction of the heart rate attempts with drug administration were not sufficient due to minor heart rate changes. By application of intravenous betablocker (esmolol) mean heart rate was only reduced from 75 ± 14 to 72 ± 12 BPM. With adenosine i.v. bolus administration, heart rate decreased further down, but did not lead to sufficient bradycardia allowing ectopic PVCs to originate, neither from the myocardium near the device or the other surrounding myocardium independent from the TECH. Therefore, AV node ablation was required. AV node ablation was performed using an irrigated ablation catheter (Intellanav Stablepoint, Boston Scientific, Marlborough, MA) and delivery of radiofrequency energy of 50 W for 60 s based on AV node localization in the 3D map. Subsequent to successful generation of total AV block (third degree) asystole occurred, requiring RV pacing, which was initiated to maintain a certain stable heart rate at 80 BPM. Afterward, RV pacing was maintained for a train of 2 min and then held or alternatively RV pacing rate was reduced down to 30 BPM to allow spontaneous beating of ectopic areas including the TECH area. After cessation of RV pacing or during bradycardic stimulation, the resulting ectopic beats, which occurred were mapped with the Orion mapping catheter, which was placed in the close proximity to the TECH device on the endocardial surface guided by fluoroscopy (Figure 5C and Figure S15, Supporting Information). Mapping analysis revealed that ectopic heart beats originated in different regions compared to regular AV nodal activation and (Figure 5D,E) further we could identify a close proximity of these areas to the TECH device in the fluoroscopy.

We aimed to confirm this observation by epicardial pace-mapping by pacing from stimulated area by TECH by a pace/sense catheter and creating an analog activation map (Movie S3, Supporting Information). These maps showed consistent QRS morphology in the surface ECG as well as an identical LAT map of the spontaneous ectopic beating compared to

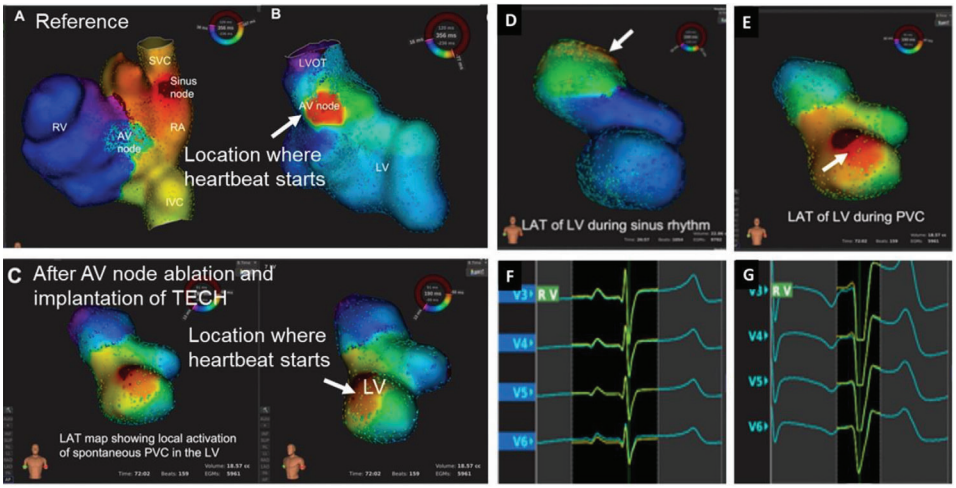

Figure 5. Cardiac pacing by electrical energy generated by TECH observed through mapping studies. 3D anatomical ultra-high-density maps including local activation time (LAT) of A) right atrium (RA) and right ventricle (RV), and B) LV with left ventricular outflow tract (LVOT) and atrioventricular (AV) node during sinus node activation. White arrows indicate where the heartbeat initiates (IVC: inferior vena cava; SVC: superior vena cava). C) LV map of spontaneous premature ventricular contractions (PVC) after AV node ablation and stimulated by electrical energy produced by the TECH. D) LAT of the LV with LV activation during sinus rhythm originating from the AV node. E) LAT map showing PVC occurring spontaneous during bradycardia from LV when stimulated by electricity produced by a TECH. F) Electrocardiogram (ECG) with narrow QRS complex from (A) and (B), and (G) wide QRS morphology in the ECG from (C).

local paced rhythm in the TECH area suggesting a TECH origin of PVCs (Figure 5F,G and Movie S4, Supporting Information).

Assumptions are justified that the electrical impulses emitted by the TECH were capable of electrical stimulation of the heart and thus contraction of the myocardium.

Hemodynamic parameters decreased during ventricular mapping from a mean arterial pressure (MAP) of 68 ± 7 to 63 ± 10 mmHg despite arterenol administration. During pacing with CNT hemodynamics and arterenol doses remained stable (MAP 61 ± 10 mmHg).

To ensure that the electrical stimulation of the heart was not caused by the mechanical irritation of the wires, the working electrode was disconnected in order to disable energy production as an intraindividual control. Subsequently there was a return to baseline heart rhythm as prior to device implantation.

3.3.2. Histological Examinations

To identify potential structural damaged to the heart, caused by the TECH, hematoxylin and eosin (H&E) and TEM examinations were performed (**Figure 6**). For histological and TEM examinations, the animal, in which cardiac stimulation was unsuccessful, was used as a control to compare the results to those with successful stimulation. For initial inspection H&E was performed to evaluate cells and tissue structure, which did not show any severe injuries such as myocardial infarction, inflammatory cell infiltration, necrosis, or loss of the normal myocardial texture (Figure 6A–F). In TEM examinations of the left atrium, septum and left ventricle mitochondrial agglomerations were visible, with swollen, but in the vast majority intact mitochondria. Myofibrils were well preserved. No differences were seen between paced and non-paced animals (Figure 6G–L). Thus, pacing with TECH had no negative effect on cell morphology.

4. Discussion

We developed a biocompatible and implantable coiled CNT energy harvester that showed good in vitro as well as in vivo performance, harvesting biomechanical energy from the beating heart. Furthermore, electrical energy from implanted TECH triggered the generation of pacemaker QRS complexes.

Twistron in conjunction with biocompatible and flexible encapsulation was able to harvest biomechanical energy from the continuous heart surface deformation. The optimal performance suitable for the target strain range of the cardiac surface could be achieved by adjusting the SI of the coiled CNT yarn working electrode.

To generate energy from mechanical linear movement, the Twistron needed to be stretched periodically. Applying the TECH to the heart, which contracts with a frequency of 60–80 BPM at rest was the obvious choice. The induced strain on the myocardium is 9%–12% in circumferential direction and 15%–23% in radial direction.[28] The LV was selected as a target area for TECH to harvest cardiac energy on its surface due to its dynamic and powerful movement with one of the thickest muscle walls in the heart.[29] As the TECH devices are soft and easily stretch no alterations to the myocardium or changes in strain pattern of the heart are expected. Li et al. investigated the best possible implantation site, in terms of maximum energy output for piezoelectrical devices on the heart.[12] Of the four different cardiac areas that were compared, namely the apex cordis, anterior wall, posterior wall, and lateral wall of the heart, the apex showed the best results. Therefore, the decision was made to implant the TECH at the apex of the left ventricle, aiming for a 20%–30% stretch of TECH. With this approach, a maximal output of 140 mV was achieved in our in vivo model from serial connection of four TECHs. Output was different for each device, and lower in the in vivo model compared to in vitro results due to the difference

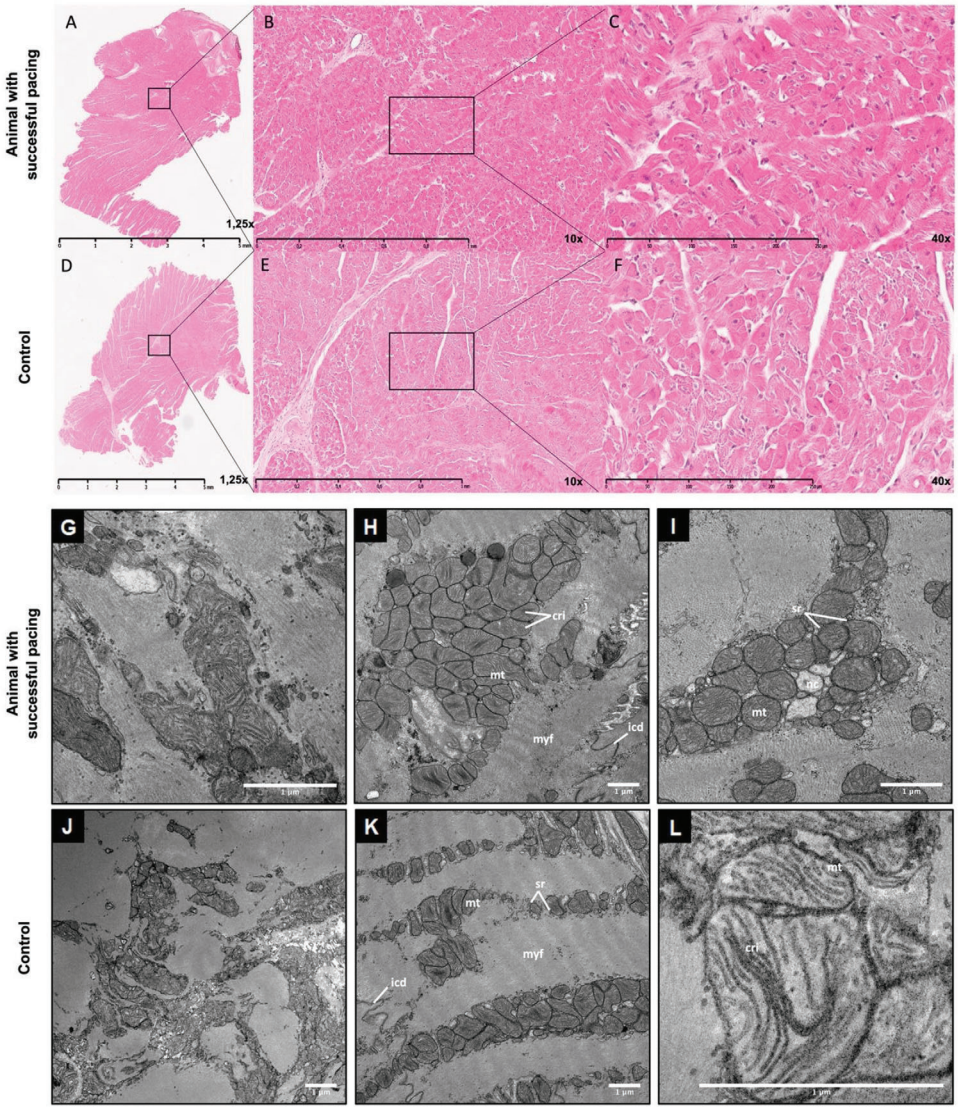

Figure 6. Investigation of intactness of the structure and tissue of the heart after TECH being implanted and heart stimulated by electrical energy from TECH. Hematoxylin and eosin (H&E) staining for cardiac cells and tissue structure of the left ventricle of the animal with A–C) successful pacing and D–F) control (A, D: 1.25× magnification, B, E: 10× magnification, C, F: 40× magnification). No cell injury was observed. G–L) Transmission electron microscopy (TEM) image of the atrium, septum, ventricle after device implantation comparing cardiac structures in a successful case (top) and control case (bottom) of cardiac pacing. G) Left atrium: Scattered mitochondrial agglomerations with fragmentation are visible. Some mitochondria are swollen and ruptured. Glycogen deposits and lipid drops are sign of modified metabolism. Swollen and cytosolic parts of muscle cells are visible. The ultrastructure of myofibrils is partly clearly visible. H) Within the septum mitochondrial clusters are visible. Mitochondria appear voluminous, dark mitochondria can be interpreted as physiological. Inner membranes of cristae are stuck together. I) TEM of the left ventricle shows mitochondrial clusters, with voluminous, round, and dark mitochondria. Few merged cristae membranes are identifiable but more physiological mitochondria are present. Some areas show cytosolic swelling and mitochondrial degradation as well as changes in tubular systems. In the control case (J)–(L), similar structures are present. Mitochondrial agglomerations are shown in the left atrium (J), with small and fragmented, sporadically perforated and swollen mitochondria. Myofibrils are difficult to recognize. K) Septum: Around the nucleus mitochondrial clusters are visible, representing a physiological state. Voluminous mitochondria show swelling without rupture. Degradation and remodeling processes in the sense of mytophagy can be seen from cristae sticking to each other. Myofibrils are well preserved. L) Left ventricle: Few clusters of mitochondria are visible. Mitochondria are fragmented with stuck together cristae membranes (mt: mitochondria; cri: Crista; Nc: nucleus; myf: myofibrils; sr: sarcoplasmatic reticulum; icd: intercalated disc).

of strains between the implantation sites. The difficulty in placing the TECH on the heart was to find the optimal LV position as well as the correct length, to ensure the TECH was able to completely relax during systole. Since four TECH devices were sutured to the relativity small porcine LV, some TECH devices were not able to perform the full stretch-and-release cycle with a 20%–30% stretch, and further research regarding more sophisticated miniaturization of the device will be able to resolve this issue.

After ensuring the continuous generation of energy by stretching TECH through cardiac motion, the wires from working and counter electrodes of TECH were inserted into the ventricle to

stimulate the heart. A stimulation from the TECH was subsequently able to generate QRS complexes (Figure 6F,G). A detailed electrophysiological mapping of the heart was performed.[7,30] This setup allowed for the comparison of QRS morphology caused by the TECH with an intentionally triggered excitation by the mapping catheter at the location of the devices, showing that both shared the same origin. The underlying principle is that a new rhythm caused by the TECH must be treated as if an ectopic rhythm source has to be localized. In consequence, the here recorded QRS complexes certainly originated from the electricity delivered from TECH. If this effect can be maintained in a long-term setting, CNT can not only be a potential source to replace batteries or at least reduce their energy consumption, but also potentially serve as an artificial cardiac pacemaker. To further exclude the possibility that the electrical excitations were caused by the manipulation of the heart itself, the wires of the TECH were torn, resulting in no further additional excitation. In addition, histological and TEM examinations confirmed, that pacing with TECH had no negative effect on cell morphology.[31]

As this study was designed as a proof-of-principle, the procedure was quite invasive regarding the access to the heart as well as number of the devices and sutures needed for fixation. The lateral thoracotomy was chosen to ensure optimal exposure of the heart and ability to observe device performance during the procedure, however in a potential clinical setting, these devices could be implanted endoscopically.

The search for alternative energy sources is a current and urgent matter in general but also for medical implants such as cardiac pacemakers, defibrillators, ventricular assist devices, neurostimulators, and insulin pumps. The current increase in lithium demand might lead to a shortage of lithium supply. Since lithium-ion batteries are the current power source for CIEDs, this could potentially pose a problem for medical care. Not only the production but also the disposal of batteries poses challenges, especially for the environment. As technology develops rapidly, power consumption of cardiac pacemakers is decreasing, opening the possibility to either be powered by Twistron or use the energy harvested from Twistron and stored in a battery. The heart as one of the most mechanically active organs presents an interesting energy source. The main task of the heart is the generation of cardiac output. However, a large amount of the energy generated by cardiac motion remains unused. Capture and subsequent channeling of this inexhaustible mechanical energy and transformation into electrical energy is therefore a desirable approach as an alternative energy source for medical implants. Biocompatible energy harvesters, as presented here, could potentially solve both problems by eliminating the need for batteries altogether, reducing the frequency of replacing them, or using the harvested energy itself for purpose of organ stimulation like a function of a pacemaker or a nerve stimulator. Following chronic animal studies must address several points: 1) performance and behavior of the device in long-term in vivo use, 2) different fixation methods, e.g., with a tissue adhesive, and 3) further optimization of the device design and improvement of the output performance to reduce the number of implanted devices.

One of our visions is the development of implantable cardioverter defibrillator and pacemaker electrodes in which the carbon nanotubes are integrated. In that way the electrodes could produce the energy needed for pacing/defibrillation by themselves through the motion of the heart or help recharge the batteries of their respective cardiac pacemakers, reducing the need for surgical battery exchange with all its caveats. Apart from that, TECH-like constructs can also serve as a sensor for the filling state of the heart in analogy to gastric sensors made of carbon nanotubes as reported previously by our group.[20]

5. Conclusion

A novel biocompatible energy harvester based on Twistron technology was developed to generate energy from mechanical contraction of the heart. TECH successfully and continuously generated electrical energy in the in vitro and in vivo experiments. Our proof-of-concept experimental setup demonstrated that pacing by TECH is feasible, opening the possibility for the development of a sustainable pacemaker based on the Twistron energy harvesting technology.

Supporting Information

Supporting Information is available from the Wiley Online Library or from the author.

Acknowledgements

The authors thank Katharina Kalka, Andreas Wissmann, Daniel Wendt, MD, Ph.D., and Ilir Balaj for their support in animal handling and anesthesia and Jaqueline Heinen-Weiler for her expert technical assistance. The authors also thank Simon Kochhäuser, MD, and Verena Marschall for their support in the electrophysiological mapping. A.O. was supported as a Clinician Scientist within the University Medicine Essen Academy (UMEA) program, funded by the German Research Foundation (DFG) and the Faculty of Medicine, University of Duisburg-Essen (Grant No. FU 356/12-2). This work was supported by the Creative Research Initiative Center for Self-Powered Actuation of the National Research Foundation and the Ministry of Science and ICT (MSIT) in Korea. The study was supported in part by the German Research Foundation (DFG) to TR (RA 969 12-1) and UHC (HE 6317/2-1).

Open access funding enabled and organized by Projekt DEAL.

Conflict of Interest

A patent application (10-2023-0133791) was filed by SJK et al. on the 6 October on "Self-powered body insertion type energy harvester."

Author Contributions

A.R., A.O., and H.K. contributed equally to this work and share first authorship. T.R. and S.J.K. contributed equally and share last authorship. Conceptualization: A.R., S.J.K., and A.O. Methodology: A.R., A.O., H.K., R.W., J.M., N.P., F.A., U.H., T.R., and S.J.K. Investigation: A.O., A.R., H.K., S.J.K., R.W., J.M., N.P., and F.A. Visualization: H.K., A.O., R.W., and J.M. Funding acquisition: S.J.K., A.R., T.R., and U.H. Project administration: A.O. Supervision: A.R., S.J.K., and T.R. Writing – original draft: A.O., H.K., and R.W. Writing – review & editing: A.R., S.J.K., and N.P.

Data Availability Statement

The data that support the findings of this study are available from the corresponding author upon reasonable request.

Disclosures

A patent application (10-2023-0133791) was filed by SJK et al. on the 6 October on "Self-powered body insertion type energy harvester."

Animal Studies Statement

The experimental protocol was reviewed and approved by the Committee on Research Animal Care, Land Nordrhein–Westfalen (Landesamt für Natur, Umwelt und Verbraucherschutz Nordrhein- Westfalen, AZ 81-02.04.2019.A465).

Keywords

biomechanical energy, carbon nanotubes, cardiac pacemaker, energy harvesting, polymer devices

Received: December 14, 2023
Revised: April 10, 2024
Published online:

[1] M. Glikson, J. C. Nielsen, M. B. Kronborg, Y. Michowitz, A. Auricchio, I. M. Barbash, J. A. Barrabés, G. Boriani, F. Braunschweig, M. Brignole, H. Burri, A. J. S. Coats, J.-C. Deharo, V. Delgado, G.-P. Diller, C. W. Israel, A. Keren, R. E. Knops, D. Kotecha, C. Leclercq, B. Merkely, C. Starck, I. Thylén, J. M. Tolosana, *Eur. Heart J.* **2021**, *42*, 3427.
[2] S. K. Mulpuru, M. Madhavan, C. J. McLeod, Y. M. Cha, P. A. Friedman, *J. Am. Coll. Cardiol.* **2017**, *69*, 189.
[3] H. Doppalapudi, J. Barrios, J. Cuellar, M. Gannon, T. Yamada, V. Kumar, W. R. Maddox, V. J. Plumb, T. M. Brown, H. T. Mcelderry, *J. Cardiovasc. Electrophysiol.* **2017**, *28*, 552.
[4] S. von Gunten, B. A. Schaer, S.-C. Yap, T. Szili-Torok, M. Kühne, C. Sticherling, S. Osswald, D. A. M. J. Theuns, *Europace* **2016**, *18*, 710.
[5] J. E. Poole, M. J. Gleva, T. Mela, M. K. Chung, D. Z. Uslan, R. Borge, V. Gottipaty, T. Shinn, D. Dan, L. A. Feldman, H. Seide, S. A. Winston, J. J. Gallagher, J. J. Langberg, K. Mitchell, R. Holcomb, *Circulation* **2010**, *122*, 1553.
[6] H. G. Mond, G. Freitag, *Pacing Clin. Electrophysiol.* **2014**, *37*, 1728.
[7] A. Ruhparwar, K. Kallenbach, G. Klein, C. Bara, A. Ghodsizad, D. C. Sigg, M. Karck, A. Haverich, M. Niehaus, *Tissue Eng., Part A* **2010**, *16*, 1867.
[8] E. W. Lau, *Pacing Clin. Electrophysiol.* **2017**, *40*, 75.
[9] K. R. Koehler, College Physics for Students of Biology and Chemistry. Cincinnati, OH, Raymond Walters College University of Cincinnati, Chapter 3, Fluids, Human Cardiovascular System **1996**.
[10] C. Dagdeviren, Z. Li, Z. L. Wang, *Annu. Rev. Biomed. Eng.* **2017**, *19*, 85.
[11] P. Nadeau, D. El-Damak, D. Glettig, Y. L. Kong, S. Mo, C. Cleveland, L. Booth, N. Roxhed, R. Langer, A. P. Chandrakasan, G. Traverso, *Nat. Biomed. Eng.* **2017**, *1*, 0022.
[12] N. Li, Z. Yi, Y. Ma, F. Xie, Y. Huang, Y. Tian, X. Dong, Y. Liu, X. Shao, Y. Li, L. Jin, J. Liu, Z. Xu, B. Yang, H. Zhang, *ACS Nano* **2019**, *13*, 2822.
[13] Q. Zheng, H. Zhang, B. Shi, X. Xue, Z. Liu, Y. Jin, Y. Ma, Y. Zou, X. Wang, Z. An, W. Tang, W. Zhang, F. Yang, Y. Liu, X. Lang, Z. Xu, Z. Li, Z. L. Wang, *ACS Nano* **2016**, *10*, 6510.
[14] G.-T. Hwang, H. Park, J.-H. Lee, S. Oh, K.-I. Park, M. Byun, H. Park, G. Ahn, C. K. Jeong, K. No, H. Kwon, S.-G. Lee, B. Joung, K. J. Lee, *Adv. Mater.* **2014**, *26*, 4880.
[15] L. Dong, A. B. Closson, M. Oglesby, D. Escobedo, X. Han, Y. Nie, S. Huang, M. D. Feldman, Z. Chen, J. X. J. Zhang, *Nano Energy* **2019**, *66*, 104085.
[16] H. Ouyang, Z. Liu, N. Li, B. Shi, Y. Zou, F. Xie, Y. Ma, Z. Li, H. Li, Q. Zheng, X. Qu, Y. Fan, Z. L. Wang, H. Zhang, Z. Li, *Nat. Commun.* **2019**, *10*, 1821.
[17] Z. Yang, S. Zhou, J. Zu, D. Inman, *Joule* **2018**, *2*, 642.
[18] S. H. Kim, C. S. Haines, N. Li, K. J. Kim, T. J. Mun, C. Choi, J. Di, Y. J. Oh, J. P. Oviedo, J. Bykova, S. Fang, N. Jiang, Z. Liu, R. Wang, P. Kumar, R. Qiao, S. Priya, K. Cho, M. Kim, M. S. Lucas, L. F. Drummy, B. Maruyama, D. Y. Lee, X. Lepró, E. Gao, D. Albarq, R. Ovalle-Robles, S. J. Kim, R. H. Baughman, *Science* **2017**, *357*, 773.
[19] T. J. Mun, S. H. Kim, J. W. Park, J. H. Moon, Y. Jang, C. Huynh, R. H. Baughman, S. J. Kim, *Adv. Funct. Mater.* **2020**, *30*, 2000411.
[20] Y. Jang, S. M. Kim, K. J. Kim, H. J. Sim, B.-J. Kim, J. W. Park, R. H. Baughman, A. Ruhparwar, S. J. Kim, *ACS Sens.* **2019**, *4*, 2893.
[21] Z. Wang, T. J. Mun, F. M. Machado, J. H. Moon, S. Fang, A. E. Aliev, M. Zhang, W. Cai, J. Mu, J. S. Hyeon, J. W. Park, P. Conlin, K. Cho, E. Gao, G. Wan, C. Huynh, A. A. Zakhidov, S. J. Kim, R. H. Baughman, *Adv. Mater.* **2022**, *34*, 2201826.
[22] M. Zhang, W. Cai, Z. Wang, S. Fang, R. Zhang, H. Lu, A. E. Aliev, A. A. Zakhidov, C. Huynh, E. Gao, J. Oh, J. H. Moon, J. W. Park, S. J. Kim, R. H. Baughman, *Nat. Energy* **2023**, *8*, 203.
[23] R. Herbert, J. H. Kim, Y. S. Kim, H. M. Lee, W. H. Yeo, *Materials* **2018**, *11*, 187.
[24] J. Heinen-Weiler, M. Hasenberg, M. Heisler, S. Settelmeier, A.-L. Beerlage, H. Doepper, B. Walkenfort, A. Odersky, P. Luedike, E. Winterhager, T. Rassaf, U. B. Hendgen-Cotta, *J. Cachexia Sarcopenia Muscle* **2021**, *12*, 933.
[25] T. Mela, J. P. Singh, *Eur. Heart J.* **2015**, *36*, 2520.
[26] M. Furrer, J. Fuhrer, H. J. Altermatt, H.-B. Ris, D. Mettler, U. Althaus, T. Carrel, *Surg. Endosc.* **1997**, *11*, 1167.
[27] Y. Nagata, V. C. Wu, Y. Otsuji, M. Takeuchi, *PLoS One* **2017**, *12*, e0180584.
[28] X. Papademetris, J. S Duncan, in *Handbook of Medical Imaging*, (Ed.: I. M. Bankman), Elsevier, Amsterdam **2000**, Vol. *2*, pp. 675–710.
[29] S. Whiteman, Y. Alimi, M. Carrasco, J. Gielecki, A. Zurada, M. Loukas, *Transl. Res. Anat.* **2021**, *23*, 100095.
[30] K. Lackermair, S. Kellner, A. Kellnar, L. M. Riesinger, R. Wakili, M. F. Sinner, K. D. Rizas, S. Fichtner, H. L. Estner, *Int. J. Cardiol.* **2018**, *272*, 168.
[31] T. Weigel, T. Schmitz, T. Pfister, S. Gaetzner, M. Jannasch, R. Al-Hijailan, S. Schürlein, S. Suliman, K. Mustafa, J. Hansmann, *Sci. Rep.* **2018**, *8*, 14545.